Frontier 2

Correlated Electrons: Science to Technology

Yoshinori TOKURA
Department of Applied Physics, University of Tokyo,Tokyo113-8656,Japan,
Joint Research Center for Atom Technology (JRCAT) and Correlated Electron Research Center (CERC)
Tsukuba,Ibaraki305-0046,Japan

Abstract

Light irradiation creates a magnet in a nonmangetic medium, and an electric or magnetic field turns a material from an insulator to a metal: such unconventional control of the state of matter is possible by exploiting *strongly correlated electrons*. Correlated electrons in solids, bear multiple degrees of freedom not only in charge sector but also in the spin and orbital sectors. Strong mutual interaction in the respective sectors, as well as cooperation/competition between the different sectors, can give rise to astonishing electronic properties/functions, such as high-temperature superconductivity and colossal magnetoresistance. Electronic and magnetic phases can be controlled by utilizing cooperative response of correlated electrons to external electric/magnetic fields, stress, and photo-excitation. The critical-state phase control is a key concept for correlated-electron technology in the future.

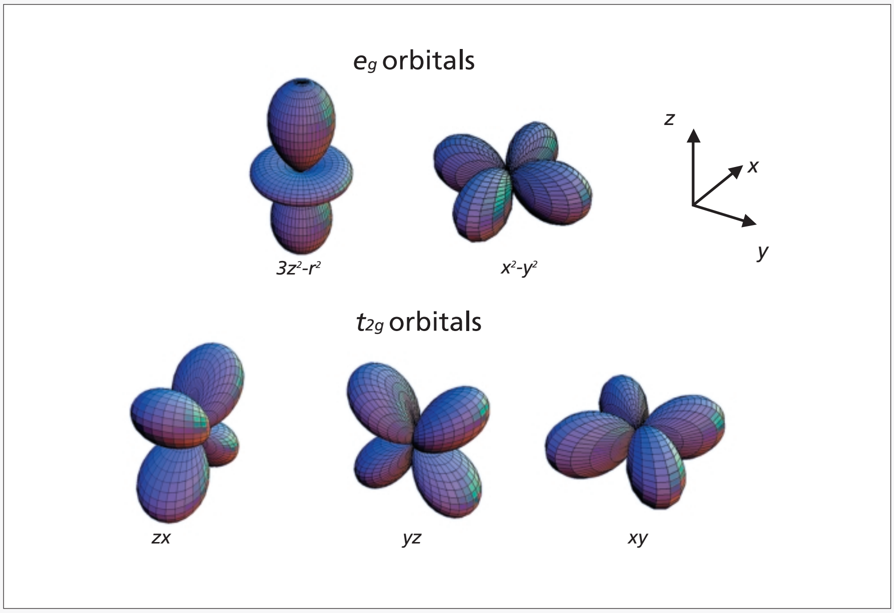

Fig. 1.
Five d orbitals. In the cubic crystal field, the five-fold degeneracy is lifted to two e_g orbitals (x^2-y^2, $3z^2$-r^2) and three t_{2g} orbitals (*xy, yz, zx*).

1. Introduction

An electron in a solid, when it is bound to or nearly localized on a specific atom, has three attributes; charge (-*e*), spin (*S*=1/2), and orbital (see the case of the d orbital in Fig.1). An orbital, which represents the electron's probability-density distribution, may be viewed as the shape of an electron in a solid. Conventional electronics utilizes the charge degree of freedom and its coupling with external electric field and light. Recent extensive R&D on spintronics, on the other hand, is directed toward the use of both the spin and the charge degrees of freedom of electrons. The *correlated-electron technology* (CET) outlined in this article will utilize all these attributes of electrons including the orbital.

In correlated electron systems, where the electron-electron Coulomb repulsion interaction is strong and electrons are almost localized or barely mobile, a naive single-particle approximation (considering a moving electron as an independent particle in the effective medium) does not hold. In this context, the concept of CET is just opposite that of single-electron manipulation: its emphasis is laid on the control of the electronic phase which interacting *many* electrons can form. The charge, spin, orbital degrees of freedom - and their coupled dynamics - can produce complex phases and phenomena such as liquid-like, crystal-like, liquid-crystal-like states of electrons, and electronic phase separation or pattern formation, as typical of complex system. The electronic/magnetic phase of a material containing correlated electrons can be controlled in unconventional ways (Fig. 2) and in an ultrafast way (at teraherz frequencies), so CET may provide a seed for a new class of electronics.

The correlation of electrons in a solid beyond the single-particle approximation typically shows up in cooperation or competition between magnetism and electrical conductance, and this has been a long-standing important (but difficult) problem in the field of condensed matter physics. Since the discovery of high-temperature superconducting (high-T_c) copper oxides, a more general interest in the Mott transition, which is the metal-insulator transition in a correlated electron system,[1] has revived peripheral fields of science as well. The high-T_c copper oxides are composed of CuO_2 sheets separated from each other by atomic barrier units called "block layers". The CuO_2 sheet is originally insulating because of the large cor-

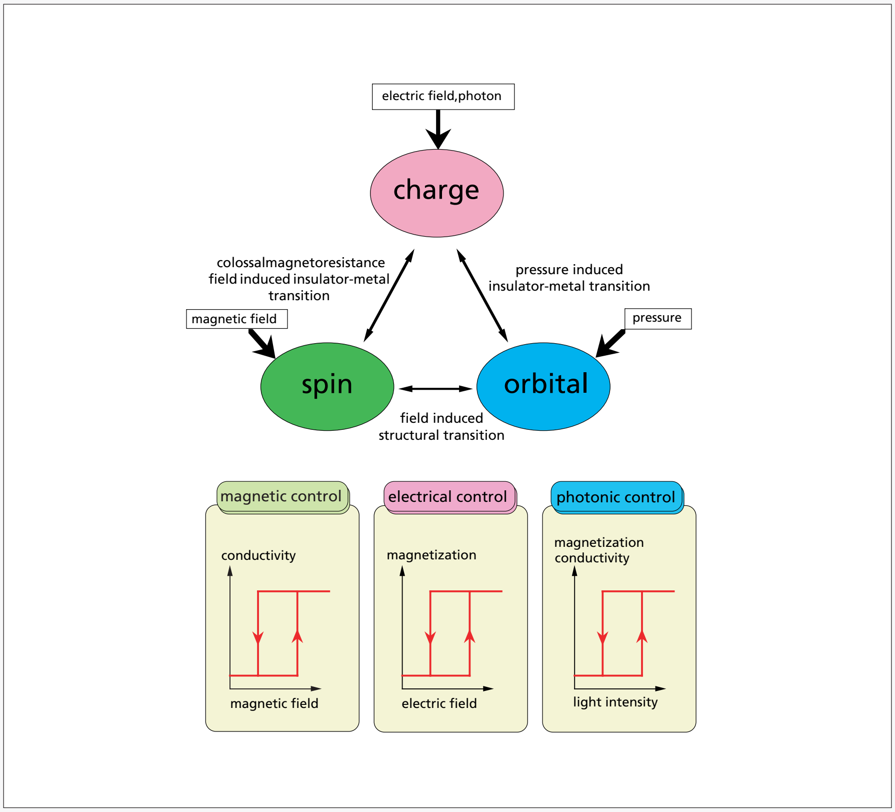

Fig.2.
Spin-charge orbital coupling for correlated d electron systems (upper) and unconventional phase control (lower).

relation effect, while possessing one conduction electron (or hole) per Cu site. This is a typical example of the Mott insulator. The high-T_c superconductivity with unconventional (perhaps d-wave) symmetry emerges upon the filling-controlled Mott transition, namely, as soon as the charge of the ionic block layer, or equivalently the change in the band filling (number of conduction electrons), causes the Mott transition. However, the strong antiferromagnetic correlation, originated in the Mott-insulating CuO_2 sheets, clearly subsists in the metallic state and this has been believed to be most relevant to the mechanism of high-T_c superconductivity.

In the course of the renaissance of the correlated-electron science during this decade, a lot of new aspects of the Mott transition phenomena have been unraveled from a modernized viewpoint.[1] One of the fruits of this renaissance was the rediscovery of the so-called colossal magnetoresistance (CMR) phenomena,[2] which is a gigantic decrease of resistance that is induced by application of a magnetic field and that is typically observed in perovskite manganese oxides. In the following of this article, we will demonstrate some examples of drastic phase changes in CMR manganites which arise from a close interplay among charge, spin, orbital, and lattice degrees of freedom.

The CET is exploiting a broad range of materials and electronic functionality in addition to the high-T_c-related and CMR-related ones. The recent advance of the fabrication technologies used to prepare thin films and superlattices has begun to produce correlated-electron junctions and atomically controlled layered structures that can be viewed as tailored correlated-electron materials. Another newly found charateristic of correlated electrons is the photonic functionality. It has also become known recently[3] that the third-order nonlinear optical susceptibility, which corresponds to the properties of two-photon absorption and the optical Kerr effect, is gigantic for some one-dimensional Mott insulators. Indeed, the third-order nonlinear optical susceptibility of these Mott insulators is comparable to or greater than that of so-far known nonlinear optical materials. These new trends in the CET research will also be dealt with in the following parts of this article.

2. Colossal magnetoresistance (CMR)

The CMR phenomena arise from the strong coupling, known as the double-exchange interaction,[4,5] between a conduction electron (e_g orbital) and local spin (t_{2g} orbital), which are both d electrons in origin but are apparently decoupled (i.e., t_{2g} electrons are localized as local spins) because of the strong correlation effect. As shown in Fig. 3(a), the spin of the conduction electron is always aligned parallel to the direction of the local spin because of the strong Hund's-rule coupling. The conduction electron cannot hop to the neighbor site when the local spins on the adjacent sites are antiparallel (antiferromagnetic). By contrast, the electron can conduct when the spin-parallel (ferromagnetic) configuration is induced thermally or by application of an external magnetic field. This atomic switching mechanism is the simplest explanation of the CMR effect. As illustrated in Fig. 3(c), when a magnetic field is applied to a perovskite-type $(Nd,Sm)_{0.5}Sr_{0.5}MnO_3$ in the antiferromagnetic (but no long-range spin-ordered) high-resistive state above the Curie temperature (T_c), the resistivity is reduced to 10^{-3} of its zero-field value and the magnetism changes from antiferromagnetic to ferromagnetic.[6]

A similar switching of the resistive state coupled with the change of spin configuration can be observed for a layered crystal of manganese oxide with bilayer-units of Mn-O sheets (Fig. 4).[7,8] In this oxide, the spin configuration between the ferromagnetic bilayer units is antiferromagnetic. The fully spin-polarized electron can therefore move freely within the layered unit but cannot hop along the interplane (c-axis) direction. But the confinement of carriers can be relaxed by the application of a magnetic field that can align all the spins in the same direction (i.e., that can cause the metamagnetic transition), resulting in the gigantic magentoresistnace effect (the right-hand panel of Fig. 4). The magnetic field strength needed for this interlayer spin alignment is less than a few hundred milliteslas, much smaller than that needed for the aforementioned atomic switching. This is viewed as the tunneling magentoresistance (TMR) effect that can usually be realized in artificial tunneling structures. Although the gigantic TMR effect can be observed only at temperatures below 100 K, the extremely large TMR value (4000%) observed under optimized condition (under pressures) may give a prospect of utilizing a half-

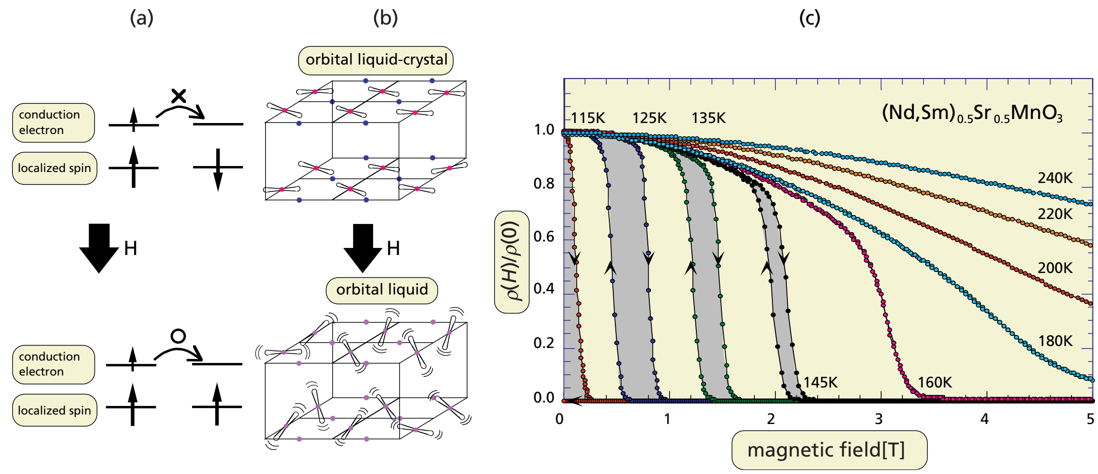

Fig.3.

(a) Spin-charge coupling for the colossal magnetoresistnace(CMR) manganite. (b) Liquid-crystal (antiferromagnetic) state and liquid (ferromagnetic metallic) state of the conduction electrons. (c) CMR observed in a (Nd,Sm)$_{0.5}$Sr$_{0.5}$MnO$_3$ crystal.

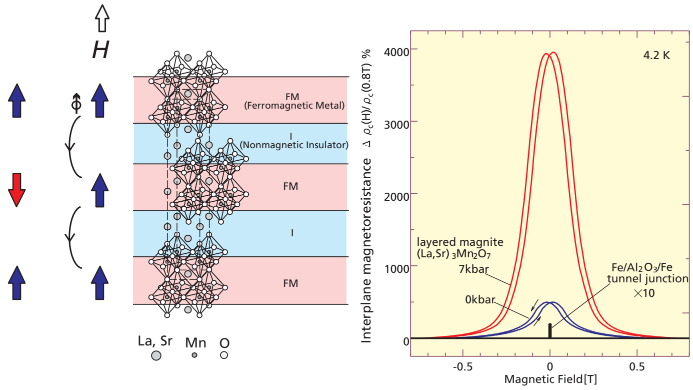

Fig.4.

Left: Layered perovskite structure viewed as a tunneling magnetoresistance system. Right: Interplane tunneling magnetoresistance for (La,Sr)$_3$Sr$_2$Mn$_2$O$_7$ crystal.

metallic (i.e., fully spin-polarized) transition-metal oxide as the component of the TMR devices.[2)]

3. Electron orbital as a control parameter

An origin of the CMR effect is thus the strong spin-charge coupling inherent in the correlated electrons. However, the physics of CMR is more complex and profound. As noted in Sec. 1, an important hidden attribute of correlated electrons is the orbital degree of freedom.[9,10)] The orbital ordering and correlation as well as their strong coupling to the spin and lattice structure is essentially important for understanding of the CMR effect. The d electron shows the five-fold degenerate states, whose respective orbitals represent spatially anisotropic electron-cloud (see Fig. 1). The crystal field lifts partially the degeneracy, but the electron orbital often behaves as a pseudo spin. It has long been well known that the orbital degree of freedom plays an important role in anisotropic magnetic interaction in transition-metal oxides[11,12)] as well as in the spontaneous lattice deformation arising from the so-called Jahn-Teller interaction.[13,14)] Recent studies of the CMR oxides have further been revealing that the dynamical or quantum fluctuation of orbital is strongly coupled with charge dynamics in the barely metallic state.[1,2,9)]

The manganese oxide (manganite) possesses the conduction electron which is accommodated in the e_g orbital state and tied by Hund's rule to the local t_{2g} spin of S=3/2. Therefore, the dominating interactions are not only the ferromagnetic double-exchange interaction, and the antiferromagnetic superexchange interaction between t_{2g} local spins, but also the exchange interaction in the orbital sector of the e_g conduction electron and the orbital-ordering induced ferromagentic superexchange interaction. The e_g orbital, which directs the surrounding oxygen sites (see Fig. 1), strongly couples with the deformation of the MnO$_6$ octahedron (Jahn-Teller interaction). For example, the $3z^2$-r^2 state tends to elongate the octahedron along the z direction, while the x^2-y^2 state tends to stretch the octahedron laterally. Conversely speaking, the uniaxial strain with respect to the MnO_6 octahedron can serve as a pseudo magnetic field on the orbital (the pseudo spin). The orbital ordering gives rise to anisotropy of the electron transfer interaction, which anisotropy either enhances or suppresses the double-exchange and superexchange interactions, thereby giving rise to complex spin-orbital coupled states.

One typical example is the case of $LaMnO_3$ or $NdMnO_3$, in which the in-plane (*ab* plane) alternate ordering of $3x^2$-r^2/$3y^2$-r^2 states realizes the in-plane ferromagnetic, while antiferromagnetic along the *c* axis, state. In the hole-doped manganites, in which the double-exchange interaction emerges with doping-dependent strength, various orbital-ordered and disordered states show up accompanying the respective spin-ordering features,[15,16] as illustrated in the top panel of Fig. 5. Let us here take the case of $Nd_{1-x}Sr_xMnO_3$. With appreciable doping on the parent compound $NdMnO_3$, the orbital order melts into a quantum-disordered state and the compound shows the ferromagnetic-metallic (F) state when $0.3<x<0.5$. With further doping ($0.5<x<0.7$), the kinetic energy of carriers decreases and the compound shows the two-dimensional metallic state with layered type antiferromagnetic (A) state.[17,18] This A state is realized because of the ferromagnetic (homogeneous) order of x^2-y^2 orbital. The overlap between the x^2-y^2 orbitals on the adjacent plane is zero in the cubic perovskite structure, and hence the electron transfer is almost prohibited along the *c* axis. This produces the antiferromagnetic coupling between the double-exchange ferromagnetic metallic sheets (*ab* planes), producing the two-dimensional half-metal sate in spite of the nearly cubic crystal structure.[18] Doping above x=0.7 further modifies the magnetic structure to the chain-type (C),[19] as shown in Fig. 5, which is described by the order of $3z^2$-r^2 orbital.

Instead of changing the carrier kinetic energy by doping, one can use the lattice strain as a biasing field on the orbital state via the Jahn-Teller interaction.[20] Figure 5(b) shows a schematic spin-orbital phase diagram for the moderately doped ($0.3<x<0.7$) manganite on the plane of the doping level vs. the uniaxial strain measured as the ratio of lattice parameter *c/a* (or almost equivalently the ratio of the apical to equatorial Mn-O bond length). The phase diagram is based on experimental results[20] obtained using the epitaxial single-crystalline films of $La_{1-x}Sr_xMnO_3$ with coherent lattice strain due to the lattice mismatching with the substrate. It is also based on the local density functional calculation on the tetragonal manganites.[16] The interplay of the doping and the strain causes the slanted phase boundaries for the F (orbital-disordered), A (x^2-y^2 ordered), and C ($3z^2$-r^2 ordered) states. As a general trend, the decrease of hole doping in this region enlarges the F state, while the increase (decrease) in the *c/a* ratio stabilizes the C (A) state as expected. In fact, thin films of $La_{1-x}Sr_xMnO_3$ (x=0.5) epitaxially grown on three different perovskite substrates show the respective ground states and the similar transport properties to those shown in the case of $Nd_{1-x}Sr_xMnO_3$ (Fig. 5(a)). Thus, near the phase boundaries, a minute perturbation, stress or carrier doping, can induce the metal-insulator or ferromagnetic-antiferromagnetic transition or both.

The orbital plays an essential role in the CMR effect itself.[2,9,21] In the highly resistive state near above the T_c (Fig. 3(c)), the orbitals of the conduction electrons are regularly arranged and directed along the same direction over some short distance. Such a dynamical ordering of charge and orbital can be viewed as "electron liquid-crystal" that is intermediate in nature between the electron crystal (charge/orbital-ordered insulator) and electron liquid (metal). The electron liquid-crystal state realized just above the Curie temperature (T_c) is antiferromagnetic in nature but is easily converted by an external magnetic field to a ferromagnetic electron-liquid state (Fig. 3(b)).

4. Unconventional phase control

In correlated electron systems with multiple degrees of freedom, unconventional phase-control like that depicted in Fig. 2 may become possible. The spin-charge-orbital cou-

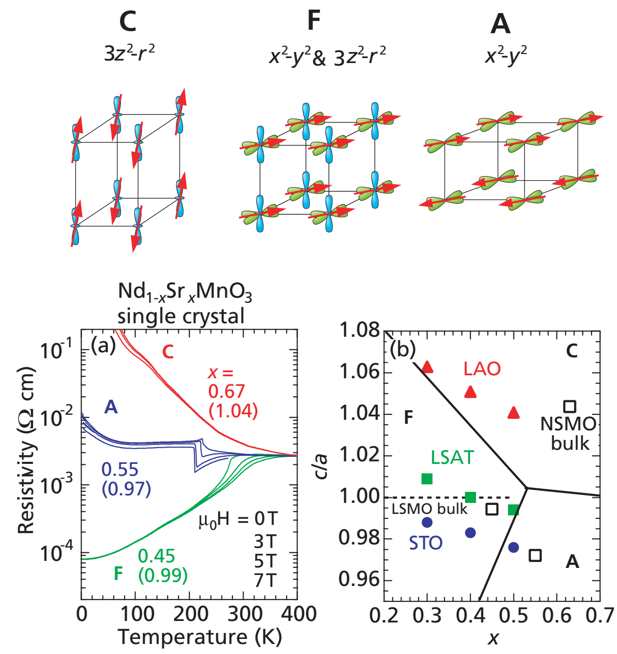

Fig. 5.

Spin-orbital phase diagram for a perovskite manganese oxide. The top panel shows the orbital and spin order in the hole-doped manganese oxides. (a) Temperature dependence of the resistivity of $Nd_{1-x}Sr_xMnO_3$ under various magnetic fields for the respective magnetic phases(F,A, and C). The number in parenthesis represents the uniaxial lattice strain(*c/a*) ratio, indicating the coupling of the magnetism to the orbital order as shown in the top panel. (b) The schematic phase diagram in the plane of lattice strain *c/a* and doping level *x*. The data labeled LAO, LSATand STO represent the results for the coherently strained epitaxial thin films of $La_{1-x}Sr_xMnO_3$ grown on the perovskite single-crystal substrates of $LaAlO_3$, $(La,Sr)(Al,Ta)O_3$, and $SrTiO_3$, respectively. LSMO-bulk and NSMO-bulk stand for the results for the bulk single crystals of $La_{1-x}Sr_xMnO_3$and $Nd_{1-x}Sr_xMnO_3$.

pling produces complex and intriguing electronic phases. The energy-scale of the dominating interactions in the correlated electron system is of the order of eV, while the competition of the phases (*e.g.* metallic vs. insulating, or ferromagnetic vs. antiferromagnetic) is usually so subtle, as described on a low-energy scale. This means that a minute perturbation as the input can cause a gigantic response accompanying the fast electronic-phase switching as the output.

The charge- and/or orbital-ordered state (electron-crystal state) is widely seen in a class of perovskite manganites and also in other transition-metal oxides.[1] This is true even for high-temperature superconducting copper oxides, which are known to show the charge-spin stripe order.[22,23] The charge ordering in the manganites accompanies the concomitant orbital ordering. The most prototypical case, called the CE type,[24-26] is realized at doping level (*x*) of 0.5 and is shown as the projection onto the *ab* plane in Fig. 6(a). In the pseudo cubic perovskite, the *ab* planes are coupled antiferromagnetically while keeping the same charge and orbital pattern. In the single-layered perovskite $La_{1-x}Sr_{1+x}MnO_4$ (x=0.5), having

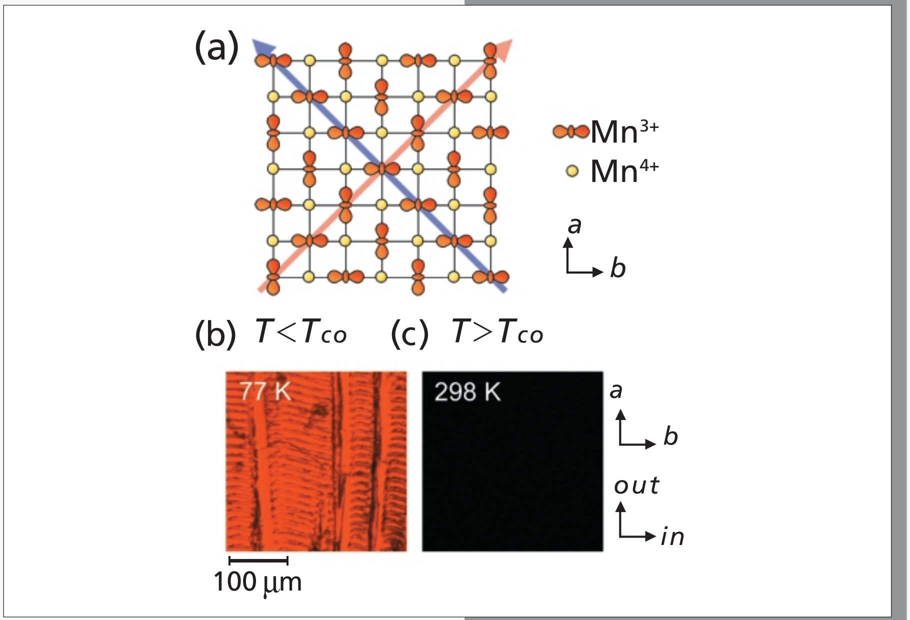

Fig.6.
(a) The orbital($3x^2$-r^2/$3y^2$-r^2) and charge order of the CE type projected on the MnO_2 sheet (*ab* plane). Lower panel: Polarization microscope image with cross polarizations parallel to *a* and *b* axes for a $La_{0.5}Sr_{1.5}MnO_4$ (x=0.5) crystal. The left bright image is for the charge/orbital ordered state at 77k . The orbital disordered state at 298K shows the isotropic optical response and hence gives the dark image.

the so-called K_2NiF_4 structure like that of the first high-temperature superconcdcutor discovered, La_2CuO_4, the same charge-orbital pattern displayed in Fig. 6 was confirmed by the resonant X-ray scattering method.[26] In this compound, the charge and orbital ordering occurs concomitantly at T_{CO}=220 K, and then the CE-type spin ordering transition sets in at T_N=150 K.[27] At higher temperatures above T_{CO} the average structure of the crystal is tetragonal, and hence the optical property is isotropic on the lateral plane. Upon the orbital ordering, the crystal is deformed to an orthorhombic one, though this deformation can hardly be detected by conventional diffraction measurements. However, the anisotropic ordering of the orbital causes a fairly large in-plane anisotropy for the optical electronic transitions, and hence in the cross-Nichol configuration of light polarization we can visualize the orbital-ordered domain.[28] The polarization microscope images for the $La_{1-x}Sr_{1+x}MnO_4$ (x=0.5) are shown in Figs. 6 (b) and 6(c). The orbital-disordered state above T_{CO} is optically isotropic in the plane, giving the extinction of cross-polarized reflection light (Fig. 6(c)), while we observe the globally bright image for the orbital ordered state below T_{CO} where the orthorhombic domain and domain walls (dark stripes) are clearly visible (Fig. 6(b)). (A periodic structure of the domains arises perhaps form the slight residual strain introduced during the crystal growth.)

The CE-type charge/orbital ordered state in the mangantie is generally amenable to application of magnetic field. Figure 7(a) illustrates a magnetic field induced insulator-metal

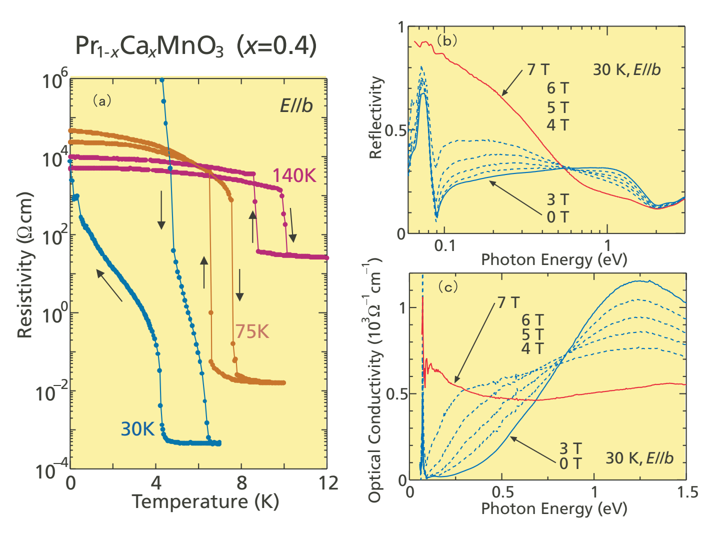

Fig.7.
(a) Melting (insulator-metal transition) of the charge/orbital-ordered state (electron-crystal state) for $Pr_{1-x}Ca_xMnO_3$ (x=0.3) by application of magnetic field at various tempeartues. Spectra of (a) optical reflectivity and (b) corresponding optical conductivity for a $Pr_{1-x}Ca_xMnO_3$ (x=0.3) crystal at 30K at various magnetic fields (in the increasing run) in the course of the insulator-metal transition.

transition for a crystal of perovskite $Pr_{0.6}Ca_{0.4}MnO_3$ that undergoes the CE-type charge-orbital ordering at T_{CO} =240 K. At low temperatures below T_{CO}, the application of magnetic field of several teslas induces the melting of charge/orbital order and changes the phase from an antiferromagnetic insulator to a ferromagnetic metal. This phase change is accompanied by a gigantic decrease of resistivity.[29] With decreasing temperature, this first-order phase transition shows an increasing field-hysteresis, indicating the occurrence of a supercooling or of a superheating effect in the field-induced melting or solidifying process. At sufficiently low temperatures, the field-induced insulator-metal transition becomes irreversible and is accompanied by a change in resistivity from above $10^{+10}\Omega$cm to $10^{-4}\Omega$cm.

The insulator-metal transition in the manganite is usually accompanied by a large change in electronic structure that shows up as a change of the optical spectrum in the infrared to visible region.[30] The magnetic field dependence of reflectivity and (transformed) optical conductivity spectra for a $Pr_{0.6}Ca_{0.4}MnO_3$ crystal at 30 K is shown in Figs. 7(b) and 7(c). The spectra show a conspicuous but continuous change with increasing magnetic field strength up to 6 T as if they prepared for the insulator-metal transition occurring around 7T. In particular, the optical gap (see Fig. 7(c)) seems to continuously decrease with increases in field strength. In accord with the insulator-metal transition at this temperature (30 K) shown in Fig. 7(a), the gap is closed at 7 T, and the metallic high-reflectivity band shows up in Fig. 7(b). The change of reflectivity spectra extends up to 3 eV, i.e. visible region. This is not a simple magneto-optical effect but should be called *magnetochromism*.

The charge/orbital ordered state or electron crystal state can also be modified by application of an electric field.[31] Figure 8 illustrates the *I-V* characteristics (representing the insulator-metal transition) at 20 K of a circuit with an manganite crystal, $Pr_{1-x}Ca_xMnO_3$ (x=0.3) subjected to various magnetic fields. The *I-V* characteristic at 4 T represents the reference curve of the ferromagnetic-metallic state, since at 4 T the charge/orbital ordered state is completely melted at this temperature. The electric-field induced change of the resistance at 0 T indicates the local insulator-metal transition due to the dielectric breakdown of the charge/orbital-ordered state. With increasing magnetic field, the breakdown threshold voltage is decreased and hysteresis is enhanced. Since the current path (metallic patch) is expected to be ferromagnetic-metallic, this phenomenon may represent the functionality of *electromagnet* that can be built in the material.

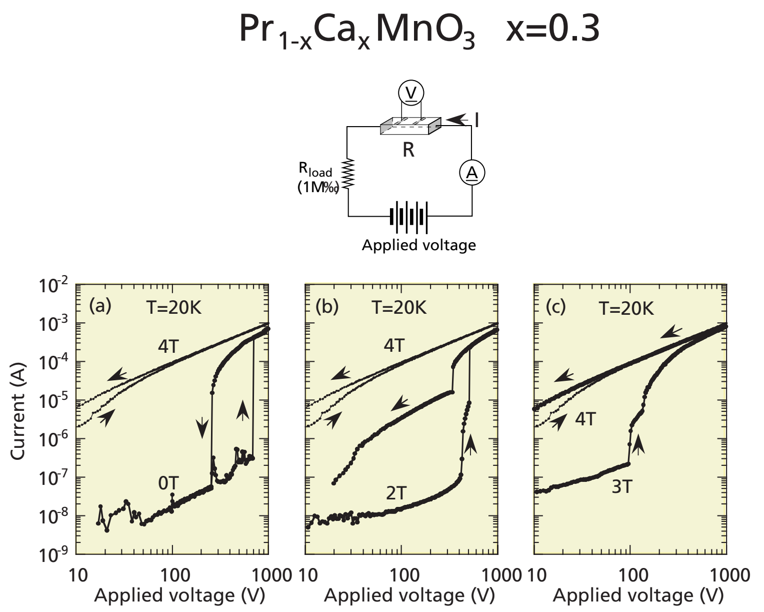

Fig.8.
I-V characteristics of the circuit with a $Pr_{1-x}Ca_xMnO_3$ (x=0.3) crystal in series (upper panel) at 20K under magnetic fields of (a) 0, (b) 2,and (c) 3T. The crystal at this temperature undergoes the magnetic field induced insulator-metal transition at 4T, and hence the curve for 4T is indicated as a reference for the bulk ferromagnetic metallic crystal.

A similar transformation from the charge-ordered insulator to the ferromagnetic metallic state can be caused by photo-excitation[323,33] or X-ray irradiation.[34] Figure 9 shows an example of the photo-induced dielectric breakdown for the same crystal, $Pr_{1-x}Ca_xMnO_3$ (x=0.3).The sample resistance across the gold electrodes with a gap of 200 µm was more than 1 GΩ at 30 K. A single nanosecond laser pulse with a photon energy well-above the charge gap (0.5 eV, see Fig. 7(c)) exteremely decreases the resistance to a few tens of ohm or generates a large persistent photoconductivity. Under a microscope, the local insulator-metal transition between the electrode gap (200 µm) is quite visible as the current path (the brightened image) in the upper panel of Fig. 9. Such a local light-induced insulator-metal transition is due to the local melting of the charge/orbital ordered state, which gives rise to a large change of the reflectivity even in the visible region as demonstrated in Fig. 7 for the case of magnetic-field induced melting. The metallic path can be sustained by passing the current. According to a pump-probe experiment[35] using 100-fs light pulses, the photo-induced melting of the charge/orbital ordered state or the local insulator-metal transition is completed within 1 ps, and is accompanied by a large change in optical reflectivity and perhaps also by the onset of the ferromagnetism. Such an ultrafast phase-control would be a great advantage in use of correlated-electron materials.

5. Tailored materials with correlated electrons

The availability of high-quality single crystals of transition-metal oxides, typically prepared by the floating-zone method, has been expediting recent researches on the physics of correlated electron systems. In addition, a recent advance in thin-film technology has provided a new tool to explore correlated-electron systems. With use of the molecular beam epitaxy (MBE) or laser ablation (laser MBE) method, thin films can be grown in a layer-by-layer mode for most of perovskite transition-metal oxides. Figure 10 shows an atomic force microscope (AFM) image of a 100-nm-thick La$_{0.6}$Sr$_{0.4}$MnO$_3$ (LSMO) film that was fabricated on a single crystal substrate of SrTiO$_3$ (STO) with the same perovskite structure by using a laser MBE method.[36] Stripes represent the 4-nm-high atomic steps corresponding to the perovskite unit cell, and the terrace region between steps shows the atomically flat region. The nearly identical atomic pattern for the surfaces of the substrate and the thin film ensures the atomically defined layer-by-layer epitaxy. A straightforward application of this technique is to the fabrication of perovskite superlattices composed of a few-u.c-thick perovskite-layers with different compositions.

A good example of the tailored materials based on the perovskite superlattice is the miltilayer system that can mimic the naturally layered magnatites with a gigantic tunneling magnetoresistance as shown in Fig.4. The superlattice may realize even a higher magnetic transition temperature than the bilayered material. For this purpose, the superlattice film can be fabricated as alternate m-units of ferromagnetic La$_{0.7}$Sr$_{0.3}$MnO$_3$ (LSMO) layers and n-units of insulating SrTiO$_3$ (STO) layers (m=1-10, n=0-5).[37] The left-hand panel of Fig. 11 shows the cross-section transmission electron-microscope image (courtesy by Dr. T. Chikyo) of the m=n=5 superlattice fabricated in a layer-by-layer mode by monitoring RHEED oscillation. The temperature variation of the in-plane resistivity in magnetic fields is illustrated in the right-hand panel of Fig. 11 for (m,n)=(5,1), (5,2), and (5,5), i.e. with varying the thickness of the insulating barrier-layer. The T_c for the (m,n)=(5,1) superlattice appears to be increased up to above 200 K, while the colossal magetoresistance (CMR) behavior is seen as in the bilayer compounds La$_{2-2x}$Sr$_{1+2x}$Mn$_2$O$_7$. However, the thick (n=5) intervening STO layer leads to the carrier localization for the thin LSMO (m=5) layer, as seen in the resistivity curve for the (5,5) superlattice. This suggests the importance of the interlayer hopping of the carriers (or electronic three-dimensionality) in producing the metallic behavior free from the localization effect.

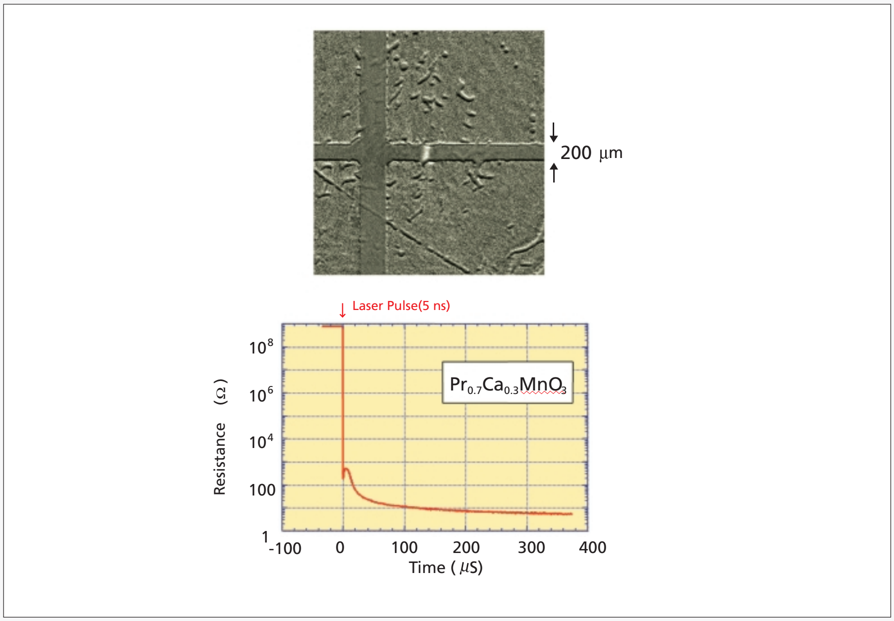

Fig.9.
The photo-induced insulator-metal transition for a Pr$_{1-x}$Ca$_x$MnO$_3$ (x=0.3) crystal at 30K. The resistance measured with the electrond gap of 200μm shows a gigantic decrease form above 1GΩ to a few tens of ohms upon the photo-excitation with a single shot of nanosecond laser (2.4 eV) pulse. Upper panel shows the image (a bright region) of the photo-induced metallic current path between the electrodes (gold). The metallic path is sustained by flowing the current.

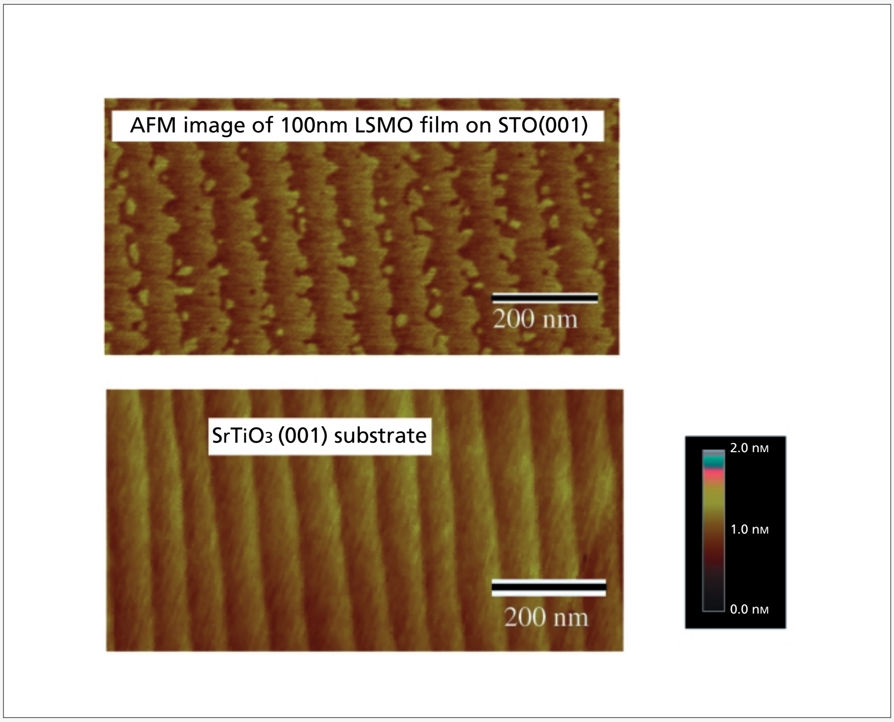

Fig.10.
Atomic force microscope (AFM) images of 100-nm-thick La$_{0.6}$Sr$_{0.4}$MnO$_3$ (LSMO) film (upper panel) grown epitaxially by laser ablation method on a single-crystal substrate (lower panel) of SrTiO$_3$ (STO).

The detailed study of this kind of superlattice films is now revealing unexpectedly rich aspects of the electronic features of the interfaces, such as charge-transfer through the interface and resultant modification of spin structure at the interfaces, and through-barrier mixing of electronic states, and relevant localization effect.[37] At the early stage in the study on the CMR manganites, a trilayer junction made of La$_{1-x}$Sr$_x$MnO$_3$ layers intervened by an insulating SrTiO$_3$ layer was fabricated as a model of tunneling magnetoresistance (TMR) device. Reflecting the half-metallic nature of

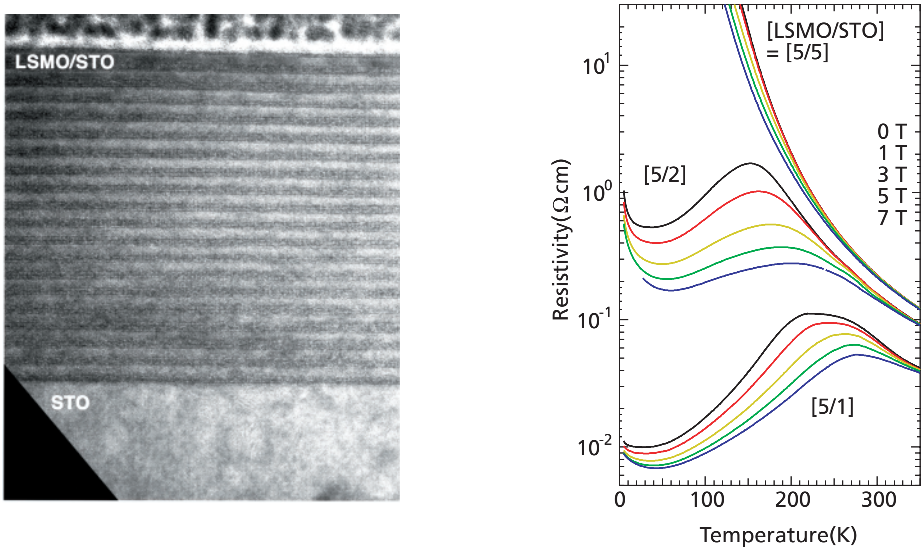

Fig.11.
Magnetoresistance properties of a supperlattice composed 20 repeated sequences of $[LSMO]_m[STO]_n$ ($LAMO=La_{0.7}Sr_{0.3}MnO_3$, $STO=SrTiO_3$; m=5,n=1,2,5). This superlattice can be viewed as tailored layered ferromagnetic compound. The left-hand panel is a cross-section image taken with a transmission electron microscope for (m,n)=(5,5) supperlattice (courtesy of Dr.T.Chikyo) .

the manganites, the TMR value is very large at low temperatures but unfortunately becomes exteremely small above about 150 K[2,38]. This is perhaps due to the spin structure modification arising from such an interface effect, which should be further pursued and will be hopefully much improved by compositional tuning of the interface region.

Let me now show the magnetotransport properties of another magnetoelectronic superlattice, those of a typical spin-superlattice composed of ferromagnetic-metallic layers ($La_{0.6}Sr_{0.4}MnO_3$; abbreviated here LSMO) and antiferromagnetic insulating layers ($La_{0.6}Sr_{0.4}FeO_3$; LSFO).[39] In Fig. 12 the properties of the the single-layer (LSMO) film are compared with those of the superlattice $[LSMO]_{10}[LSFO]_3$ (suffixes indicate the numbers of repeated unit cells (u.c.) of the respective layers.) LSFO shows the G-type (alternate spin-up and spin-down) antiferromagnetic state. The superlattice whose properties are shown in Fig. 12 was epitaxially grown on a (100) substrate of perovskite $SrTiO_3$ with coherent strain. Therefore the interface of originally ferromagnetic LSMO and antiferromagnetic LSFO layers shows a spin frustration irrespective of the sign of the magnetic coupling at the interface. The much enhanced resistivity of the superlattice at zero field is due not only to the confinement effect of the charge carriers in the thin (10-u.c.) LSMO layer but also to the frustration-induced modification of the spin structure at the interface (perhaps from ferromagnetic to spin-canted antiferromagnetic). This was confirmed by examining the LSFO-layer thickness dependence of the resistivity and magnetic response for the superlattice while keeping the thickness of LSMO constant (10 u.c.): with increasing LSFO layer thickness, the resistivity increases and the net magnetization of the constituent LSMO layers decreases. As shown in Fig.12, an extremely large magnetoresistance effect was observed for this (10,3) superlattice down to the lowest temperature, whereas the LSMO single-layer film showed the conventional MR only around T_c. This difference between the two kinds of films can be accounted for by the field-induced modification of the canted spin structure near the interface (see the lower panel of Fig. 12). The original spin canting near the atomic interface reduces the thickness of the conducting region of the LSMO layer, but the effective thickness of the conducting region is increased when an external field forces the canted spins into ferromagnetic alignment.

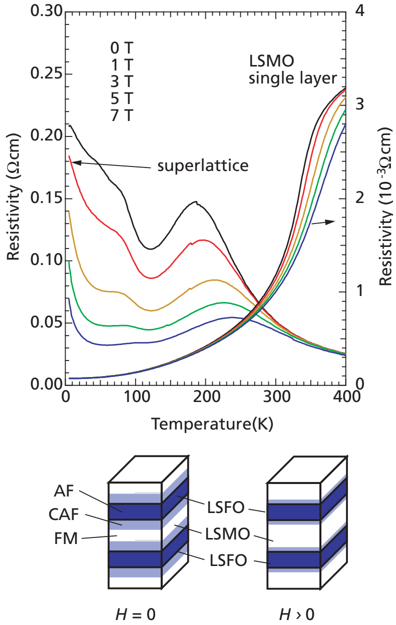

Fig.12.
Magnetoresistance properties of the superlattice containing 20 repeated sequences of $[LSMO]_{10}[LSFO]_3$ ($LAMO=La_{0.6}Sr_{0.4}MnO_3$ and $LSFO=La_{0.6}Sr_{0.4}FeO_3$) in comparison with those of LSMO (thick) films . The bottom panel depicts the mecanism of the colossal magnetoresistance of the supperlattice:The canted afntiferromagnetic (CAF) region near the LSFO/LSMO interface is converted by an external magnetic field to a ferromagnetic (FM) one, increasing the effective thickness of the FM region as a wave-guide for the spin-polarized carriers.

The perovskite superlattices can be composed of a variety of combinations of layers with various compositions, and not only the charge gap and spin structure but also the orbital state of the constituent layers play important roles in determining the properties of the supperlattices. The charge transfer across the interface, which transfer is affected by the

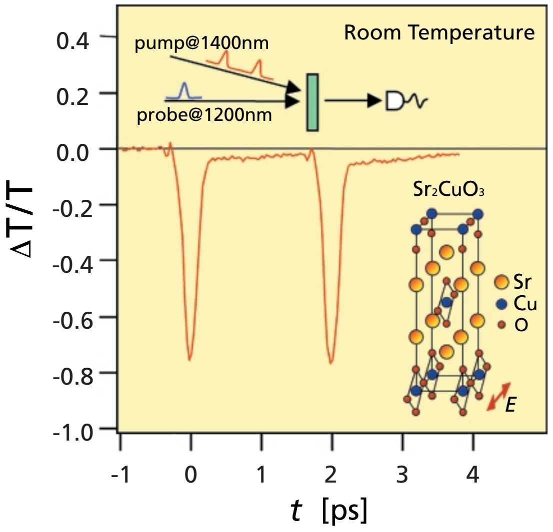

Fig.13.
Photo-switching (modulation of optical transmittance) experiment at room temperature using a Sr_2CuO_3 crystal (as a strong two-photon absorber) ,which is a prototypical Mott insulator with Cu-O chain structure. Pump and probe pulses were 100fs in duration and a train of the two pulses separated by 2ps causes the distict optical switching.

chemical potential as well as by the orbital-spin state, is particularly important, because it affects the spin structure at the interface and hence the transport property. It is not so easy at the moment but quite a rewarding task to conjecture and design electronic and magnetic properties of superlattices composed of the transition-metal oxide perovskites. This emerging research field assures an abundant gold mine for new correlated-electron materials.

6. Photonic functionality of correlated electron systems

So far little known but potentially useful characteristic of the correlated electron systems is their role in nonlinear optical (NLO) materials and photo-switching device materials. In the Mott insulator, a charge gap is formed as a result of the large on-site Coulomb energy, termed *U*. Occasionally, and in particular for the transition-metal oxides such as nickelates and cuprates, the actual charge gap is formed not between the *U*-split bands (lower and upper Hubbard bands) of d electrons, but between the oxygen (or halogen) filled p-band and upper Hubbard (unoccupied) d-band and is termed a charge-transfer gap.[40] The charge gap transition with the *p-d* character bears a large transition dipole but occurs well above 1eV, and hence there is still a large transparent window in the near-infrared region, which is the wavelength region used in optical-fiber communication systems.

Up to now, materials with large third-order NLO susceptibility have been sought in the family of one-dimensional semiconductors like organic conjugate polymers and polysilanes (linear Si-polymers).[41] This is partly because the NLO susceptibility is favored by the linear extension of the excited state wave functions as well as the large oscillator strengths of the essential-state transitions, such as those between the ground state and the first excited state and between the first and higher excited states. In this context, there is an important class of one-dimensional systems with correlated electrons among transition-metal oxide and halide materials. In these systems there is strong *p-d* electron hybridization that enhances the transition dipole moments between the above-mentioned essential states, while the electron correlation effect keeps the appreciable charge gap magnitude. In fact, a recent systematic study[3] of one-dimensional charge-transfer insulators such as halogen-bridged Ni complexes and Sr_2CuO_3 has shown that there is a large transition dipole between the first and second excited states which are almost energetically degenerate. This situation can produce a gigantic third-order optical nonlinear susceptibility ranging from 10^{-8} - 10^{-4} esu in the resonance energy region.

Figure 13 demonstrates the fast photo-switching, at room temperature, of near-infrared lights by using a typical one-dimensional charge-transfer insulator, Sr_2CuO_3 (see the inset for its structure).[42] This compound is a one-dimensional analog of a high-temperature superconductor parent compound La_2CuO_4: it contains Cu-O chains instead of CuO_2 sheets. When the polarization of two incident light beams is parallel to the Cu-O chain and the sum of the two photon energies is 2-3 eV, strong two-photon absorption (one of the third-order NLO properties) occurs. Figure 13 shows the transmittance change of this compound at 1200nm due to the two-photon absorption that is induced with two pump pulses with 2ps apart in a train. The use of the two-photon absorption that occurs in the conventional semiconductors is not suitable for all-optical switching devices because the accumulation of two-photon generated electron-hole pairs becomes a big obstacle to the fast recovery of the ground sate. In Fig. 13, however, the tail component of the transmittance change seems small enough. This is perhaps because the optically silent high-energy spin excitations provide an effective recovery-channel to the ground-sate. This would be a great advantage of the correlated electron system in their use in NLO devices. Thus, the use of the correlated-electron materials is a quite promising approach to explore new NLO materials and ultrafast (THz) optical switching devices.

7. Correlated-electron technology

We have seen several examples of intriguing electronic phases produced by strongly correlated electrons. This article has focused on the manganites, but another promising family of correlated-electron are, needless to say, the high-temperature supercondcuting copper oxides (cuprates) with perovskite-related structures similar to those of the mangantites. Both the CMR manganites and the high-temperature superconducting cuprates will be major element systems in correlated-electron technology (CET). There are, however, also many other compounds we might use for CET. Those compounds, including some organic molecular compounds, have various instabilities of charge/spin/orbital ordering and are thus on the verge of the electronic phase transformation. In many of those compounds, exotic spin and/or orbital textures, e.g., a chiral spin state and an incommensurate charge/spin/orbital stripe, show up, which would provide another CET functionality. The use of those correlated-electron materials would be based on the concept of the phase-control of complex electronic states. Because of an inherently large energy-scale of the electronic parameters in correlated electron systems, external stimuli can be expected to cause a gigantic and ultrafast response in electrical, magnetic, optical, and dielectric properties. In conclusion, let me summarize the future subjects of CET research:

[1] critical-state phase control of correlated electrons
[2] tailoring new materials phases by superlattice technology
[3] fabrication of junctions and interfaces of correlated-electron system
[4] searching for photonic materials with strong electron correlation
[5] devising new principles for CET

Among them, new principles for CET would be highly desired, that can coherently describe complex quantal phases, utilize those quantal phase dynamics, and substantiate their application in quite a different way from prevailing single-electron technology.

The author would like to thank N. Nagaosa, M. Kawasaki, K. Miyano, M. Kuwata-Gonokami, H. Okamoto,T. Ogasawara, K. Terakura, Y. Tomioka, T. Kimura, and M. Izumi for their help in writing this article and for enlightening discussions. The works presented here were done at JRCAT under the support of the NEDO and in the COE research project at Department of Applied Physics (Butsuko), University of Tokyo under the support of the Ministry of Education.

JSAP

References

1) For a review, see M. Imda, A. Fujimori, and Y. Tokura, Rev. Mod. Phys. **70**, 1039 (1998).
2) For a review, see, for example, Colossal Magnetoresistive Oxides, edited by Y. Tokura (Gordon&Breach Science Publishers, London, 2000) and references therein.
3) H.Kishida et al., Nature, June 22 issue (2000).
4) C. Zener, Phys. Rev. **82**, 403 (1951).
5) P. W. Anderson and H. Hasegawa, Phys. Rev. **100**, 675 (1955).
6) H. Kuwahara, Y. Tomioka, A. Asamitsu, Y. Moritomo, and Y. Tokura,Science , **270**, 961 (1995).
7) T. Kimura, Y. Tomioka, H. Kuwahara, A. Asamitsu, M. Tamura, and Y. Tokura, Science **274**, 1698 (1996).
8) T. Kimura, Y. Tomioka, A. Asamitsu, and Y. Tokura, Phys. Rev. Lett. **81**, 5920 (1998).
9) For a review, see Y. Tokura and N. Nagaosa, Science **288**, 463(2000).
10) K. I. Kugel and D. I. Khomskii, Sov. Phys. JETP 52, 501 (1981).
11) J. Kanamori, J. Phys. Chem. Solids, **10**, 87 (1959).
12) J. B. Goodenough, Magnetism and Chemical Bond (Interscience, 1963).
13) H. A. Jahn and E. Teller, Proc. R. Soc. A**161**, 220 (1937).
14) J. Kanamori, J. Appl. Phys. Suppl. **31**, 14S (1960).
15) R. Maezono, S. Ishihara and N. Nagaosa, Phys. Rev. B **58**, 11583 (1998).
16) Z. Fang, I. V. Solovyev, K. Terakura, Phys. Rev. Lett. **84**, 3169 (2000).
17) H. Kawano et al., Phys. Rev. Lett. **78**, 4253 (1997).
18) H. Kuwahara, T. Okuda, Y. Tomioka, A. Asamitsu, and Y. Tokura, Phys. Rev. Lett. **82**, 4316 (1999).
19) R. Kajimoto et al., Phys. Rev. B **60**, 9506 (1999).
20) Y. Konishi et al., J. Phys. Soc. Jpn. **68**, 3790 (1999).
21) S. Shimomura, N. Wakabayashi, H. Kuwahara, and Y. Tokura, Phys. Rev. Lett. **83**, 4389 (1999).
22) J. M. Tranquda et al., Nature **375**, 561 (1995).
23) S. A. Kiverson, E. Fradkin, and V. J. Emery, Nature **393**, 550 (1998).
24) E. O. Wollan and W. C. Koehler, Phys. Rev. **100**, 54 (1955).
25) J. B. Goodenough, Phys. Rev. **100**, 564 (1955).
26) Y. Murakami et al., Phys. Rev. Lett. **80**, 1932 (1998).
27) B. J. Sternlieb, J.P. Hill, U. C. Wildgruber, G. M. Luke, B. Nachumi, Y.Moritomo and Y. Tokura, Phys. Rev. Lett. **76**, 2169 (1996).
28) T. Ishikawa, K. Ookura, and Y. Tokura, Phys. Rev. B **59**, 8367 (1999).
29) Y. Tomioka, A. Asamitsu, H. Kuwahara, and Y. Tokura, Phys. Rev. B **53**, R1689 (1996).
30) Y. Okimoto, Y. Tomioka, Y. Onose, Y. Otsuka, and Y. Tokura, Phys. Rev.B **57**, R9377 (1998).
31) A. Asamitsu, Y. Tomioka, H. Kuwahara and Y. Tokura, Nature **388**, 50(1997).
32) K. Miyano, T. Tanaka, Y. Tomioka and Y. Tokura, Phys. Rev. Lett. **78**, 4257 (1997).
33) M. Fiebig, K. Miyano, Y. Tomioka, and Y. Tokura, Science **280**, 1925 (1998).
34) V. Kiryukhin et al.,Nature, **386**, 813 (1997).
35) M. Fiebig, K. Miyano, Y. Tomioka, and Y. Tokura, to be published.
36) M. Izumi et al., Appl. Phys. Lett. **73**, 2497 (1998).
37) M.Izumi, M. Kawasaki, and Y. Tokura, unpublished.
38) Z. J. Sun et al., Appl. Phys. Lett. **65**, 3266 (1996).
39) M. Izumi et al., Phys.Rev.B **60**, 1211 (1999).
40) J. Zaanen, G. A. Sawatzky, and J. W. Allen, Phys.Rev.Lett. **55**, 418 (1985).
41) For a review, see *Nonlinear Optical Properties of Organic Molecules and Crystals*, edited by D. S. Chemla and J. Zyss (Academic Press Inc., London, 1987).
42) T. Ogasawara et al., to be published (cond-mat/0002286).